NDT&E International 154 (2025) 103386

Contents lists available at ScienceDirect

NDT and E International

journal homepage: www.elsevier.com/locate/ndteint

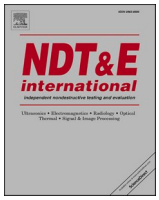

SNR equalization in non-contact resonant ultrasound spectroscopy measurements

Muhammad Tayyib *, Linas Svilainis

Electronics Engineering Department, Kaunas University of Technology, Kaunas, LT-51368, Lithuania

ARTICLE INFO

Keywords:
Non-contact resonant ultrasound spectroscopy
Signal to noise ratio
Spread spectrum signals
Spectral losses compensation

ABSTRACT

It is proposed to replace the single pulse excitation with spread spectrum signal of programmable spectral shape in non-contact resonant ultrasound spectroscopy (NC-RUS). Bandwidth can be improved by pushing the signal energy towards high loss frequencies. It has been demonstrated that not just signal spectrum but also noise spectral density are irregular, therefore not only signal spectrum but SNR has to be equalized. The benefit of SNR-equalized signals in RUS is the improved SNR over broader bandwidth which results in better inverse solution convergence. Arbitrary position, and width pulses (APWP) sequences performed best. It was demonstrated that unipolar APWP signals can be used to obtain the acceptable performance of spectral shaping. Use of unipolar excitation allows for simpler electronics. While −20 dB bandwidth in case of pulse excitation was 480 kHz, APWP excitation produced 670 kHz bandwidth. The proposed was compared against pulse, linear frequency modulation (LFM) and nonlinear frequency modulation (NLFM) signals in NC-RUS measurements of plant leaf and polycarbonate plate. In leaf measurements, bias error in density estimation was 2 % with APWP signals while LFM resulted in 45 % and pulse in 60 % error. The polycarbonate sample velocity estimation error for polycarbonate sample using APWP signal was 0.2 %, while LFM was 10 times higher (2 %); density estimation error for APWP was 3 %, but LFM resulted in 36 %, NLFM error was 22 %, pulse excitation resulted in 12 % error.

1. Introduction

Ultrasonic techniques are widely used for the determination of material properties, providing a valuable insight into structural properties of material. Equipment is low cost, small size, uses no ionizing radiation. Sample properties can be determined using the structure resonances in resonant ultrasound spectroscopy [1–5]. However, the predominant approach still involves the contact-based [6] or immersion [7] techniques. An air-coupled ultrasound is preferred in cases where physical contact or liquid coupling are not suitable because the wetting may alter the material properties. The examples of such case are paper [8], cardboard [9], composite prepreg [10], drugs [11], oxidizable materials [12] or plant leaves [13]. Non-contact resonant ultrasound spectroscopy (NC-RUS) is a technique for the simultaneous velocity and thickness (also ultrasound attenuation and density) estimation of a thin plate sample [14–16] by fitting a thickness resonance model [17]. It was successfully demonstrated for membranes, films [8,18], facemasks [19], solid plates [16], plant leaf [13] measurement. Nonetheless, the air-coupled ultrasound has challenges of its own: large signal losses due to acoustic impedance mismatch [21], and attenuation in the air [22,23]. The solution for impedance mismatch is to use a several quarter wavelength matching layers [24–26]. Development of air-coupled transducer technologies [27,28] allowed for significant bandwidth and sensitivity improvement, but the lack of materials for the last matching layer is limiting the attainable bandwidth [21] and signal to noise ratio (SNR). The center frequency of the air-coupled transducers must be kept low due to attenuation in the air. Since the transduction bandwidth of the ultrasonic transducer is a fraction of its center frequency, the available bandwidth is not sufficiently broad. Additionally, quarter wavelength matching produces nonuniform transmission spectrum.

Commonly, NC-RUS is carried out using a single pulse or spike signal [16,29,30] because it can be generated using simple circuit, its response is easy to gate and interpret. However, pulse signals are highly inefficient, because narrow pulse must be used for broadband excitation, which results in low signal energy and therefore, lower SNR is obtained. Moreover, energy of the pulse or spike is concentrated at low frequencies (which do not pass the transducer) so less energy is left at high frequencies. SNR can be improved by averaging a large amount of signal

* Corresponding author.
E-mail address: muhammad.tayyib@ktu.edu (M. Tayyib).

https://doi.org/10.1016/j.ndteint.2025.103386
Received 12 November 2024; Received in revised form 25 January 2025; Accepted 9 March 2025
Available online 10 March 2025

waveforms [16,29,30], but such an approach is unacceptable if conditions are varying.

Measurements from several transducers with different center frequency are usually combined in NC-RUS to solve the bandwidth issue [8,12,16,18,19,29,30], but single transducer can be used if sufficient SNR is achieved by use of spread spectrum signals. Spread spectrum (SS) signals [31], especially rectangular ones [32], are more energy-efficient, exploit the power source capabilities in full extent. Yet, the standard ones, in particular chirp (linear frequency modulation, LFM) and phase shift keying sequences (PSK) do not have spectral shape control ability therefore cannot effectively compensate for the spectral losses. It was already demonstrated that standard LFM signal spectral shape can be altered by using amplitude modulation (AM) [33]. Yet, such excitation does not exploit the full power source capabilities and requires digital-to-analog (DAC) converter, linear amplifiers, which are complex and not energy-efficient and demand more complex electronics. The solution is programmable spectral shape signals, like nonlinear frequency modulation (NLFM) [32,33] or arbitrary pulse width and position (APWP) [35] signals. It was demonstrated in Refs. [36,37] that excitation spectral shape can be altered in order to compensate for the transduction losses and increase the available signal bandwidth at the reception's end. However, there are two remaining problems. Bipolar rectangular pulse sequences were used for excitation in Refs. [36,37]. Bipolar excitation is more efficient in spectral content management, but it requires more complex electronics than unipolar excitation. Unipolar excitation would be preferred, aiming at equipment size, weight, and cost. Secondly, a common assumption is that the noise spectrum is flat i.e., white, but this is not the case for piezoceramic transducers. The piezo element of the transducers is working in thickness resonance; therefore, response is similar to that of the resonant tank [38]. Application of backing and matching layers introduces new resonances. Therefore, the impedance of the ultrasonic transducer varies with the frequency [39] and the output noise of the reception amplifier is not white [40]. The novelty of the approach proposed here is to use the unipolar excitation and alter the transmitted spectrum in such a way that uniform SNR is ensured over wider bandwidth. Moreover, previous publications [36,37] used compensation for contact or immersion transducers, which already possess wide bandwidth, but losses compensation was never tried for air-coupled NC-RUS. Moreover, previous publications used the bipolar excitation which provides more flexibility in spectral shape programming. Use of the unipolar excitation simplifies the excitation electronics, but the control over the signal spectra is more complicated.

This paper proposes the following contribution to NC-RUS:

i) single pulse excitation is replaced by spread spectrum signal APWP of programmable spectral shape;
ii) SNR is improved, there is no need for averaging, which results in more stable results;
iii) spectral shape optimization, differently from Refs. [36,37], involves not just signal losses but also noise spectrum, smooth SNR is obtained over whole bandwidth;
iv) unipolar APWP sequences are used so simpler excitation electronics can be used.

2. NC-RUS for plate in air

The through-transmission NC-RUS uses two measurements: free propagation (Fig. 1 bottom) and with sample inserted (Fig. 1 top). The distance between transmitting and receiving transducers should be the same in all measurements.

Two 650 kHz center frequency air-coupled transducers (designed and manufactured by CSIC, Spain) were used to demonstrate the NC-RUS operation. The transmission AC response $T(\omega)$ (refer Fig. 2 for the example spectrum of the grape (*Vitis vinifera*) leaf) is obtained by taking the ratio between sample and calibration signals in frequency domain [17]:

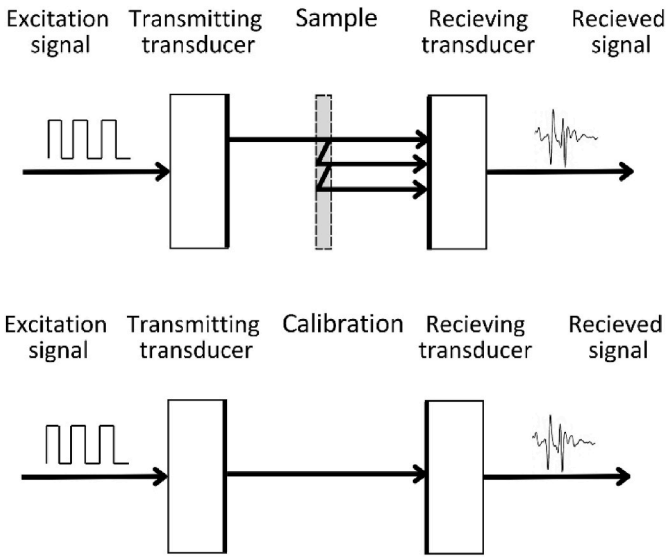

Fig. 1. Resonant ultrasound spectroscopy measurement types: sample (top) and calibration (bottom).

$$T(\omega)=\frac{S_{RXS}(\omega)}{S_{RXC}(\omega)}, \tag{1}$$

where $S_{RXC}(\omega)$ is the calibration signal spectrum and $S_{RXS}(\omega)$ is the sample signal spectrum.

It can be noted that multiple reflections within the leaf produce resonance at 780 kHz. Propagation of the ultrasonic signal through the leaf can be described by Brekhovskikh's model [17]:

$$T'(\omega)=\frac{-Z_1Z_2}{-2Z_1Z_2\cos(k'h)+j\left(Z_1{}^2+Z_2{}^2\right)sin(k'h)}, \tag{2}$$

where Z_1 is the acoustic impedance of the air Z_2 is the acoustic impedance of the sample, h is the sample thickness, k' is the complex wave number:

$$k'=\frac{\omega}{c_2}-j\alpha, \tag{3}$$

where c_2 is the ultrasound velocity in the sample, α is the acoustic attenuation in sample, defined as:

$$\alpha=\alpha_0\cdot\left(\frac{f}{f_0}\right)^n, \tag{4}$$

f_0 is the normalization frequency that is used as resonant frequency of transducer i.e., 650 kHz.

The impedances Z_1 *and* Z_2 can be obtained using velocity $c_{1,2}$ and density $\rho_{1,2}$:

$$Z_1=c_1\cdot\rho_1, \& \; Z_2=c_2\cdot\rho_2, \tag{5}$$

where, c_1 is the ultrasound velocity in the air and ρ_1 is the air density.

Then sample signal can be obtained from calibration signal as:

$$S_{model}(\omega)=R(\omega).T'(\omega)e^{j\omega h/c}, \tag{6}$$

where additional component, $e^{j\omega h/c}$ is to account for the signal shift due to the air replacement with the sample within thickness h.

Sample parameters $\mathbf{x}$=(h, c_2, n, ρ_1 and α) can be estimated by solving the inverse problem of equation (6). The inverse solution is obtained by minimizing the difference between the simulated s_{mod} and experimentally measured s_{RXS} signals:

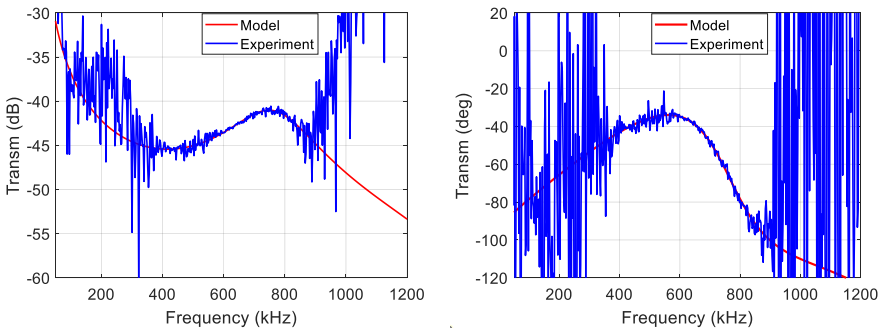

Fig. 2. Transmission response of experimentally measured *Vitis vinifera* leaf: magnitude (left) and phase (right) response.

$$\mathbf{x} = \arg\ \min \sum_{i=1}^{N} \left(\frac{s_{mod}(\mathbf{x})_i - s_{iRXS}}{s_{iRXS}} \right)^2, \tag{7}$$

where N is the signal waveform length in samples.

3. Problem definition

This section is dedicated to detailed explanation of the problems addressed in this paper.

3.1. NC-RUS demands wide bandwidth and high SNR

Figs. 3 and 4 below are used to indicate how sample parameters are affecting the transmission spectra. The experimentally obtained parameters of *Vitis vinifera* leaf (see Fig. 2) were used in equation (2). Each parameter varied up and down by significant margin individually to reflect how particular parameter affects the spectral shape.

From the analysis of the results above it can be concluded that high dynamic range (high SNR) and broad bandwidth are required in order to cover all possible parameters values. A spectral valley can become hidden in noise which would result in bias errors in parameters estimation. It can be assumed that spectral peak can fall out of passband, but bias errors can be kept low if sufficient SNR is ensured for the rest of spectra. Transmission spectrum in Fig. 2, obtained by using pulse signal (blue curve), demonstrates that good SNR is ensured only within relatively narrow bandwidth (around 650 kHz). The reason is that the transmission peak is at 650 kHz (refer Fig. 5 red). The resonant nature of piezo element and matching layers used for bandwidth and sensitivity improvement produce the nonuniform frequency response. The signal level can be increased with spread spectrum LFM (chirp) excitation signal (Fig. 5 black).

Still, it can be noted that the received signal spectrum varies with frequency and does not cover the sufficient frequency bandwidth.

3.2. Flat signal spectrum does not correspond to flat SNR

The signal spectrum can be flattened, and bandwidth increased by using the APWP signals [35] of programmable spectra (refer Fig. 6).

Compensation is at the expense of some signal energy loss within the passband in exchange of signal energy increase at passband edges (note APWP improvement at 900–1000 kHz range in Fig. 6). Yet, another problem lies in the complex nature of the transducer impedance [39]. It is the common assumption that receiving amplifier output noise is flat i.e., white, and only signal spectra needs flattening. However, this is not the case with piezoceramic, especially air-coupled transducers. The reception preamplifier noise, when driven by the same 650 kHz transducer, is presented in Fig. 7. The output noise and preamplifier gain AC response were measured first. Then results were converted to the input noise voltage spectral density (NVSD) using technique presented in Ref. [39].

It can be noticed that noise spectral density varies across the passband of the transducer: at 400 kHz it is 2.65 nV/$\sqrt{\text{Hz}}$ and at 830 kHz it is 3.45 nV/$\sqrt{\text{Hz}}$. Therefore, despite received signal spectrum was flattened, the resulting SNR is not flat (see Fig. 8).

It can be concluded that the air-coupled transducers are more complex than immersion [36], or contact [6], due to their more complicated construction and narrower bandwidth. Therefore, flattening the transmission response does not provide flat SNR, required for NC-RUS measurements.

3.3. Bipolar excitation is less demanding for electronics

Excitation signal defines the output waveform. The best results are obtained using arbitrary waveform excitation signals [34] but require digital-to-analog converters (DAC) and linear analog amplifiers, resulting in costly, expensive, and inefficient equipment. Compared to the arbitrary waveform, rectangular signals are generated just by using the switches, which remove the need for DAC and linear amplifiers. Bipolar excitation was used in previous publications for transmission response

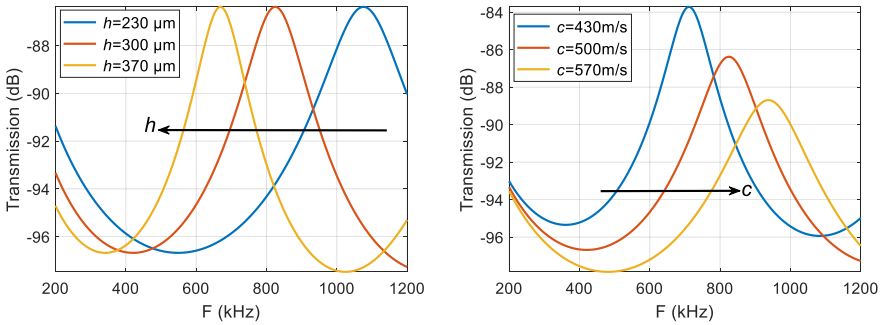

Fig. 3. Simulated transmission responses when thickness (left) or velocity (right) vary.

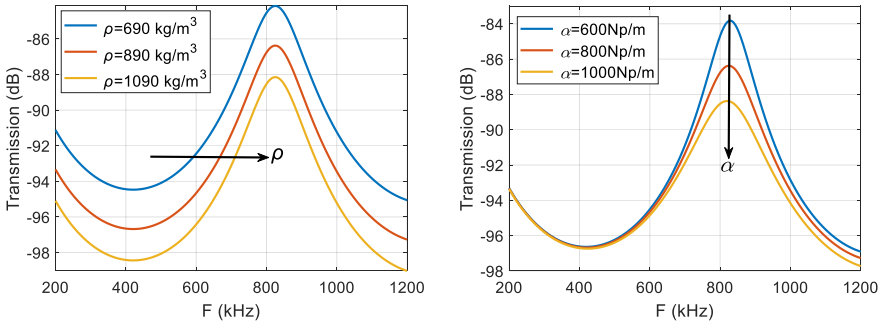

Fig. 4. Simulated transmission responses when density (left) or attenuation (right) vary.

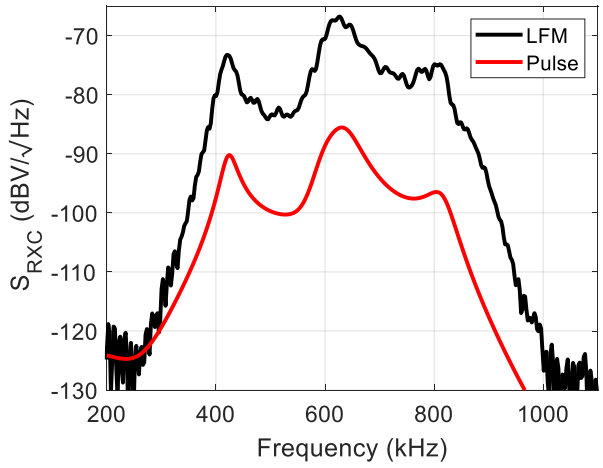

Fig. 5. The magnitude spectrum of the received signal when pulse(red) is used as excitation signal and LFM (black) signal for air-coupled transducer.

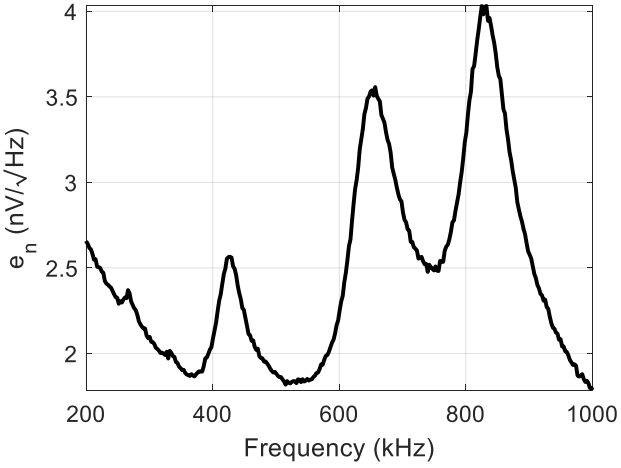

Fig. 7. Preamplifier input NVSD when connected to receiving transducer.

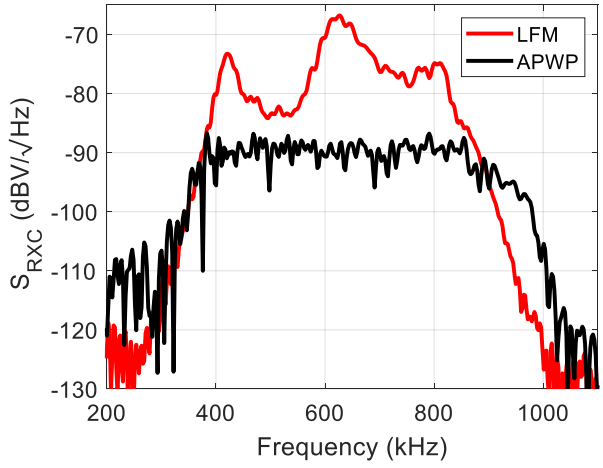

Fig. 6. The magnitude spectrum of the received signal when air-coupled transducer is excited by LFM (red) and losses-compensating APWP signal (black) signal.

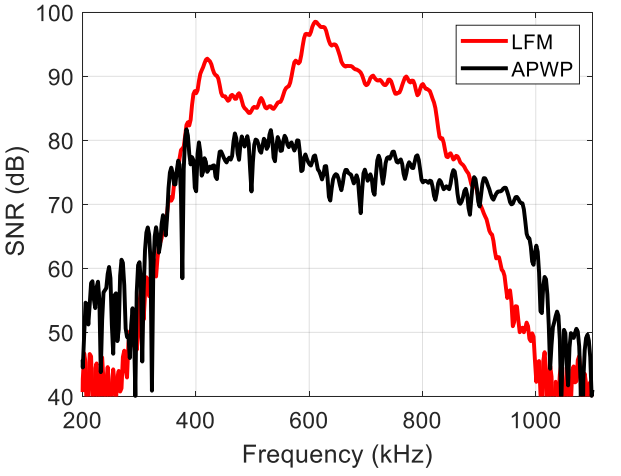

Fig. 8. Received signal SNR when transducer is excited by LFM (red) and losses compensating APWP (black) signal.

optimization [36,37]. Bipolar excitation provides more flexibility in spectral shape programming, but equipment is still complex. A unipolar excitation is proposed in this work for APWP signals production to further simplify the excitation electronics, improve its efficiency and cost. Duration and position in time of every individual pulse can be altered in APWP signals (Fig. 9).

However, the unipolar signals produce a spectral ripple due to the convolution with *sinc* function. Also, such excitation has less control over signal spectra. Therefore, the optimization process is more complicated.

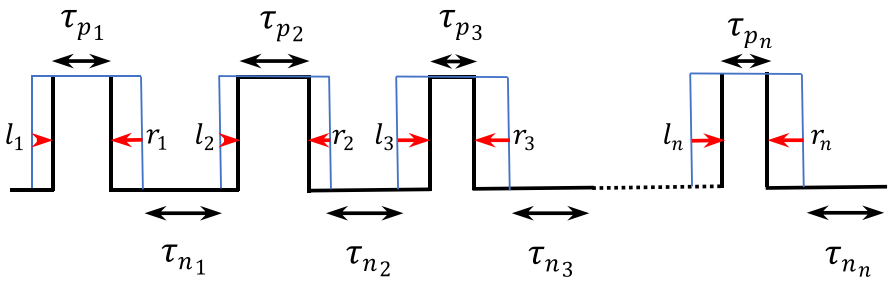

Fig. 9. Unipolar APWP signal.

4. Proposed solution: flat SNR using unipolar excitation

There are two problems: i) the transmission response between two transducers is not flat and ii) the output noise of the reception amplifier is not flat. Then it is proposed here that it is the SNR that should be used in APWP signal optimization. The best results would have been obtained if compensation for sample measurement was used. However, this would mean that every new measurement requires new APWP signal optimization. As an alternative, it was proposed to compensate the calibration setup SNR. Then APWP optimization can be done just one time. The corresponding compensation path can be seen in Fig. 10.

Compensation for spectral losses is only done for the components which influence the measurements, i.e., electronics and transducers. Essential, that SS signals can be made long thus giving the flexibility to improve the SNR without implicating the bandwidth of the signal. Then, excessive SNR can be sacrificed in exchange for spectral losses compensation in order to flatten the SNR AC response.

Derivation of APWP signal starts with NLFM signal production. Optimization is done for direct propagation (calibration) measurement by examining the SNR flatness within the selected frequencies range.

In order to derive the NLFM signal, the signal transmission AC response is measured first, by exciting with broadband (300–950 kHz) 100 μs chirp (LFM). The multiple waveforms ($M = 1000$) of the signal s_{RXC} present at reception amplifier output are averaged in time domain and resulting averaged signal is transformed into frequency domain using discrete Fourier transform (DFT):

$$S_{RXC} = \sqrt{\frac{2 \times DFT\left(\sum_{i=1}^{N} s_{iRXC}\right)^2}{N \times fs \times M}}. \tag{8}$$

Next step is to measure the noise spectral density. The measurement is carried out with no signal transmitted. M measurements are transformed into frequency domain using discrete Fourier transform (DFT) and averaged power-wise to obtain the NVSD:

$$e_n = \sqrt{\frac{2 \times \sum_{i=1}^{N} |DFT(s_{iRX0})|^2}{N \times fs \times M}}, \tag{9}$$

where, f_s is the sampling frequency and N are number of samples.

SNR is thereafter used for the derivation of compensation path:

$$SNR_C = \frac{S_{RXC}}{e_n}. \tag{10}$$

The compensation function is obtained as follows:

$$\kappa(f) = \frac{|W(f)|}{|SNR_C(f)|}, \tag{11}$$

where $W(f)$ is the spectral windowing function used to control the bandwidth. Tukey window with decay 0.3 and 300–950 kHz range was used. The compensation function was derived from SNR presented in Fig. 7.

It must be noted that compensation function is obtained for excitation signal, LFM in particular. The desired excitation signal spectrum then is:

$$S_{TXdes}(f) = \kappa(f)|S_{TX}(f)|, \tag{12}$$

where $S_{TX}(f)$ is the excitation signal spectrum. Such a spectrum can be obtained by NLFM signal [38], where energy of each spectral component is determined by rate of change of instantaneous frequency. NLFM could be derived by first arriving to frequency-time relationship:

$$\tau(f') = \int_0^{f'} \left(\kappa(f)|^2\right) df. \tag{13}$$

equation (13) needs to be inverted into $f(\tau)$, which is required for instantaneous phase calculation. Inversion is done by resampling the non-uniform grid τ (Fig. 11, right):

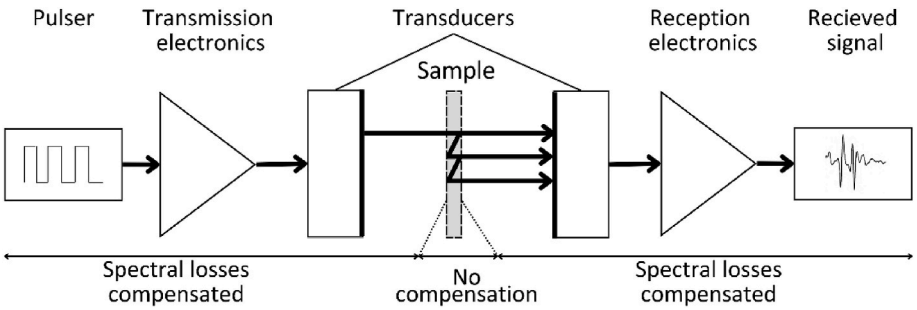

Fig. 10. SNR compensation signal path excludes the sample.

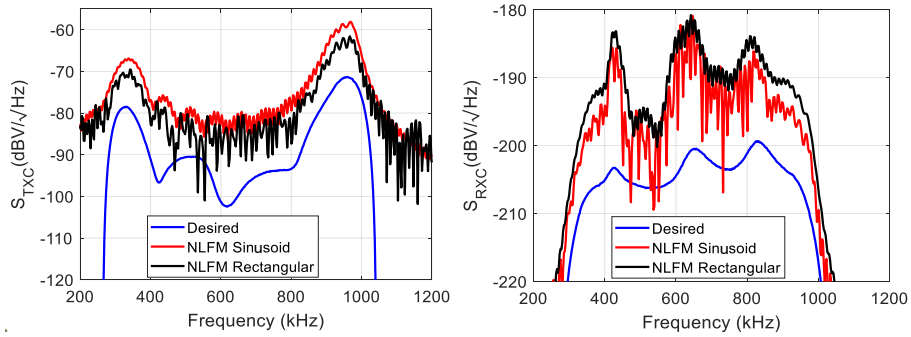

Fig. 11. Comparison of transmitted (left) and received (right) signals spectra for the desired (blue), sinusoid NLFM (black) and rectangular NLFM (red) signals after spectral losses compensation. Note that the desired spectral shape was not obtained.

$$\tau(f') \xrightarrow{Interp} f'(\tau). \tag{14}$$

Phase θ, is obtained by integration over the instantaneous frequencies:

$$\theta(t') = 2\pi \int_0^{t'} f'(t)dt, \tag{15}$$

Then the required NLFM signal is obtained:

$$s_{TXNLFM}(t) = sign(\sin\theta(t)). \tag{16}$$

NLFM signal is effective in utilizing the output range of excitation amplifiers, because envelope is constant over time. Conversion to the unipolar form (sign operation) is to produce the rectangular waveform, which facilitates more simple excitation electronics. Received signal S_{RXC} spectra for the desired (± 1 V) and unipolar NLFM (+1 V) signals are presented in Fig. 11. The important thing to note is that compensation increases the bandwidth, but the desired spectral shape was not obtained.

The usual way to correct the situation is to apply the proper envelope modulation and revert to sinusoidal signal. This would mean turning to AM-NLFM signals [34], but these are based on arbitrary waveforms, thus, require bulky, and costly system in the form of linear amplifiers and generators. On the contrary unipolar waveforms are preferred due to better exploitation of voltage swing dynamic range and efficiency (note the magnitude difference). The APWP sets [35] are proposed for final spectrum shaping. These signals offer spectral adjustment, by changing the pulse durations and placement in time.

Yet, APWP signals require optimization, so their derivation is a lengthy process. In order to speed up the optimization process, a numerical model of the system transmission response of calibration measurement was developed. Numerical model for calibration measurement was based on infinite impulse response (IIR) filter. Filter was developed as a close simulated approximation using the experimental measurement results. Transducers were placed at 32 mm distance and excitation using 700 ns duration, 50 V amplitude pulse; 1000 waveforms were averaged to get sufficient SNR of calibration signal S_{RXCexp}. The 8th order IIR filter was used. Such low order is not sufficient to simulate the 32 mm propagation distance, but higher order filter will become unstable. Therefore, IIR filter was combined with subsample delay operator $e^{-j\omega ToF}$ with delay equal to time-of-flight (ToF'):

$$T_{sys} = \frac{S_{RXCexp}}{(V_{HV}.P.e^{-j.\omega.ToF'})}, \tag{17}$$

where S_{RXCexp} is experimentally measured calibration signal, P is the excitation signal, described as sequence of 1's or 0's, V_{HV} is the amplitude of the excitation signal, T_{sys} is the system (including the excitation electronics, transmitting, and receiving transducer) transmission AC response, ToF' is to simulate the delay of propagation in air and partially-delay in transducers and electronics. ToF' was estimated as cross correlation peak between S_{RXCexp} and P with cosine subsample interpolation [40]. T_{sys} was then inverted to get IIR filter coefficients a',b' (using Matlab *invfreqz* function). The coefficients a',b' were used for particle swarm optimization (PSO) constrains (upper and lower bounds) derivation:

$$LB(a,b) = (a',b')/2 \;\&\; UB(a,b) = (a',b')*2. \tag{18}$$

The remainder energy of the simulated and experimentally measured subtraction was used as a convergence criterion to further optimize the a and b coefficients:

$$y = \arg\ \min \sum_{i=1}^{N} \left(\frac{s_{RXCsim_i} - s_{RXCexp}}{s_{RXCexp}} \right)^2, \tag{19}$$

where s_{RXCsim} is the simulated calibration signal produced as:

$$s_{RXCsim} = IIR(P,a,b).e^{-j.\omega.ToF}, \tag{20}$$

ToF was estimated as a cross-correlation peak between $IIR(P,a,b)$ and P with cosine subsample interpolation [40]. Optimized parameters a,b and ToF were stored as the calibration signal propagation model coefficients. The IIR filter was implemented as a second order section (SOS) to improve stability.

The conversion of SNR-compensated NLFM signal into APWP signal was started from direct assignment (APWP= NLFM). Signals received were obtained by simulation (using equation. (20)) to speed up the optimization process. The $SNR_{Ci}(f)$ was obtained from excitation signal P_i, generated in the ith iteration. SNR spectral flatness ξ was evaluated within the desired passband f_{min}-f_{max}:

$$\xi_i = \sqrt{\frac{\int_{f_{min}}^{f_{max}} \| SNR_{Ci}(f)| - |\overline{SNR}_{Ci}(f)\|^2 df}{|\overline{SNR}_{Ci}(f)|}}. \tag{21}$$

The SNR flatness was regulated by adjusting the individual APWP pulses duration and position in time.

The optimization process is described as:

1. Transmit the original APWP signal and estimate the initial spectral flatness ξ_0. The APWP signal contains N rectangular pulses, each L_n samples long ($n = 1, \ldots, N$);
2. Resize the nth pulse (starting from the first), transmit it and estimate the new spectral flatness ξ_{in}. Resizing (Fig. 9) involves two secondary loops, outer one which adjusts the pulse's left side by $l = -L_n/2, \ldots, 3L_n/2$ and inner one adjusts the right side by $r = -3L_n/2, \ldots, L_n/2$;
   a Resize the nth pulse left size by l;
      i Resize the nth pulse right side by r;
      ii Transmit the resized pulse and use the received signal to calculate the SNR spectral flatness ξ_{lr};

b Select the best contender from $l \times r$ ξ matrix (the one that provides minimum ξ) and set $\xi_i = \min_{l,r} \xi_{lr}$;
3. Replace the nth pulse with the one with best ξ and repeat 2 for the next pulse updating $n = n+1$ until $n = N$;
4. Calculate the spectral flatness reduction of the ith iteration $\Delta\xi_i = \xi_i - \xi_{(i-1)}$. Repeat 2 until $\Delta\xi_i$ lays below certain threshold or until maximum iterations are reached.

The pulse width reduction of APWP results in envelope modulation. Also, the interpolation errors introduced from equation (14) were reduced due to pulse position shifting.

The result can be evaluated by comparing the SNR spectral flatness in Fig. 12. It can be seen that APWP produces the best SNR spectral flatness compared to pulse, LFM, and NLFM. The results displayed were all generated using the same peak amplitude for all transmitted signals.

It must be noted that SNR-equalized APWP provides improved spectral losses compensation at frequencies beyond 900 kHz and below 380 kHz (note the arrows indicating the improved passband for APWP). The −20 dB bandwidth for pulse was 480 kHz, meanwhile APWP was able to achieve 670 kHz bandwidth. On the other hand, NLFM provides similar bandwidth, but the SNR spectrum is not as flat. Additionally, APWP provides improved SNR. The effect of such compensation on NC-RUS is evaluated in the next section.

5. Evaluation of the compensation effect on NC-RUS

The performance of the proposed compensation scheme was evaluated both by simulation and experimentally. Simulation used grape (*Vitis vinifera*) leaf analytical model equations (2)–(6). Experimental investigation used 2.045 mm polycarbonate plate. Bias errors of the parameter's estimation were evaluated. Such double choice has a reason: i) it is difficult to measure the actual thickness of the leaf because it is fragile, ii) density measurement is also complicated due to complex leaf anatomy, iii) it is a living organism and therefore all its properties would vary during the experiment time, iv) reference values for density, velocity and attenuation are not available (may vary from leaf to leaf) and v) leaf properties are affected by circadian rhythm, watering, lighting, and temperature. On the contrary, polycarbonate reference values are available from broad literature sources [41,42]. Therefore, results obtained can be compared against these values.

5.1. Simulation of Vitis vinifera measurement

The only parameters that can be validated by mechanical measurements are the thickness and the density. It is difficult to measure the actual sample thickness because leaves are fragile and living organisms exhibit varying properties over time. Density measurement is also complicated due to complex leaf anatomy. Furthermore, leaf properties will change due to circadian rhythms, watering, lighting, and temperature. Therefore, it was decided to validate the technique performance on *Vitis vinifera* using a numerical simulation.

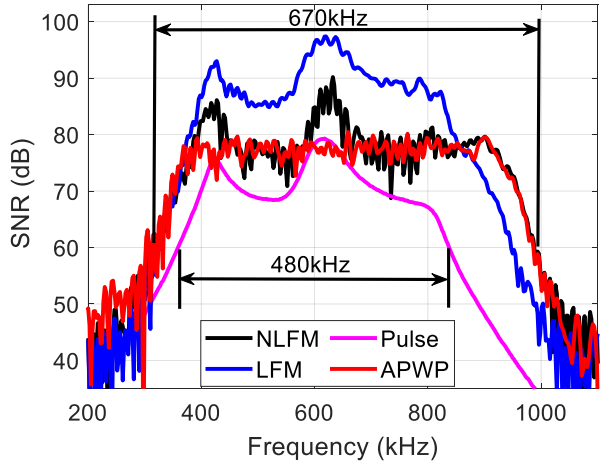

Fig. 12. Received SNR comparison. Note that SNR is flat only for APWP signal. Bandwidth was improved for NLFM and APWP signals.

Calibration signal was produced by model already described in section 4, equations. (17)–(21). It includes full system model: transmission electronics, transmitting transducer, air propagation, receiving transducer and reception electronics.

Sample signal was obtained by using experimentally obtained values $\alpha = 800$ Np/m, c = 315 m/s, $h = 250$ μm, $\rho = 890.89$ kg/m^3 in equations (2)–(5).

Signals obtained were added to a random noise. 1000 noise waveforms were produced first with random colored (statistically following Fig. 7 spectral shape) Gaussian noise. Then signals and noise were added to simulate actual measurements. A total of 1000 waveform sets were obtained for each of the four excitation signals (pulse, LFM, NLFM and APWP) which were corrupted by colored noise. Large measurements set was required to reduce the random errors, because bias error was used in performance evaluation.

Next, NC-RUS inverse solution (equations (1)–(5)) was obtained using PSO with objective function (equation (7)). The estimated sample parameters were averaged and then compared with actual (best available estimate) ones to obtain the bias errors. The fitting process was achieved using constrained boundaries with lower bound as half of the average estimated parameters and upper bound as double of the average estimated parameters (equation (18)).

The transmission response of four excitation signals, pulse, LFM, NLFM, and APWP, are displayed in Fig. 13.

Spectral response analysis provides a valuable insight into the performance of each signal. Pulse is the simplest excitation signal with smallest energy; thus, its SNR performance is the worst, which can be expected (Fig. 13 (top left)). It resulted in 400–820 kHz coverage bandwidth. LFM, on the other hand, provided the highest energy with coverage from 380 kHz to 880 kHz and SNR is the best in this range compared to all signals (Fig. 13 (top right)). However, it was assumed that SNR flatness is more important than large energy at frequencies where transduction losses are small. Therefore, energy was pushed into stopband for NLFM and APWP signals (refer Fig. 12). NLFM and APWP provided acceptable SNR at broader bandwidth of 300–950 kHz (Fig. 13 (bottom left and right respectively)), compared to LFM. Yet, small distortions are visible in the passband of NLFM and APWP spectra as energy was removed from this area.

5.2. Experimental polycarbonate plate measurements

The experimental setup used a dedicated data acquisition system (Fig. 14). The system includes two air-coupled transducers with center frequency of 650 kHz, which are mounted at a fixed distance of 35 mm. It also includes a sample holder which also serves a hood and the waveguide. High voltage power source, transmission and reception electronics, filters, an analog-to-digit converter, temperature and humidity sensor, wireless communication electronics are also embedded. More details can be found in Ref. [20].

A 2.045 mm thin polycarbonate sample was placed between transducers. Acquisition system was augmented with linear actuator which was used for automated sample insertion (sample measurement) and removal (calibration measurement). 1000 calibration and sample waveforms were collected in sequence. Such large measurements were required to reduce the random errors of measurement, because bias errors were used in performance evaluation. Experiment was conducted in a thermally insulated box of polystyrene. Consequently, ambient temperature variance was minimized: registered temperature range inside the box during whole experiment time ranged from only

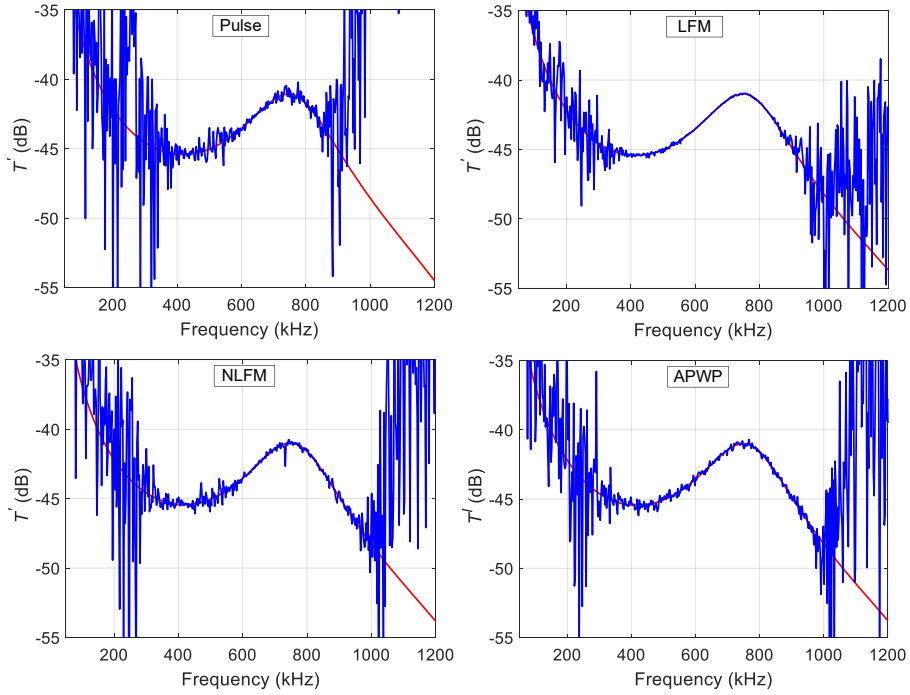

Fig. 13. Transmission magnitude for *Vitis Vinifera* leaf in case of different excitation signals: pulse (top left), LFM (top right) NLFM (bottom left) and APWP (bottom right).

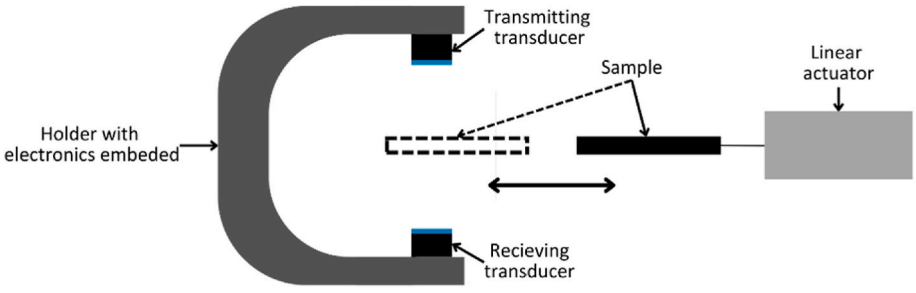

Fig. 14. Experimental setup used for the evaluation of polycarbonate sample by using air-coupled ultrasonic data acquisition system.

24.13 °C–24.30 °C (an approximate variation of only 0.704 %).

The transmission response obtained by taking ratio of sample to calibration signal in frequency domain is presented in Fig. 15. The experimental transmission response (blue) is compared to the inverse solution (red) result for each of the four excitation signals (pulse, LFM, NLFM and APWP).

The actual thickness of the sample is 2.045 mm and estimated ultrasound velocity is 2240 m/s, this corresponds to resonance peak at 537 kHz. It can be noted that inverse solution results for pulse and LFM signals differ from experimentally obtained transmission so large bias errors can be expected for these signals. Acceptable SNR in case of pulse excitation is ensured only for 450–620 kHz. For LFM excitation 400–700 kHz range is covered reliably, 380–930 kHz range is covered by NLFM. Best coverage is by APWP, 380–1000 kHz. Final judgement should be based on sample parameters (sample thickness, density, ultrasound velocity and attenuation) estimation performance presented in next section.

5.3. Results analysis

Sample parameters were estimated by NC-RUS inverse solution, resulting in 1000 values of sample thickness, density, ultrasound velocity and attenuation. Then each 1000 values for each parameter were averaged. This value was considered as measured value. Parameters values (α = 800 Np/m, c = 315 m/s, h = 250 μm, ρ = 890.89 kg/m^3) used in simulation were considered as reference values in case of *Vitis vinifera* sample. Reference values for thickness and density were derived from caliper and weight measurements (h = 2.045 mm, ρ = 1193.6 kg/m^3), attenuation and ultrasound velocity values (α = 43.5 Np/m, c = 2240 m/s) were taken from Ref. [42] in case of polycarbonate sample. Relative bias errors were obtained by taking the ratio of absolute error to reference value.

Bias errors for sample attenuation α estimation are shown in Fig. 16 for *Vitis vinifera* (left) and polycarbonate (right) samples.

It can be noted that the largest *Vitis vinifera* sample attenuation error is in the case of LFM excitation (16 %), followed by pulse (12 %) and NLFM (5.5 %). Results obtained using SNR-optimized APWP signals have the lowest error of 1 %. In experimental polycarbonate measurements, APWP also performs best with only 17 % bias error compared to pulse (27 %), LFM (30 %) and NLFM (26.5 %) signals.

Ultrasound velocity c bias errors are shown in Fig. 17 for *Vitis vinifera* (left) and polycarbonate (right) samples.

Ultrasound velocity estimation bias error for *Vitis vinifera* sample is largest in case of NLFM excitation signal (7 %), followed by pulse (4.5 %) and LFM (2.4 %) signals. Excitation by APWP signal results in the lowest error of 0.3 %. The velocity estimation errors for polycarbonate

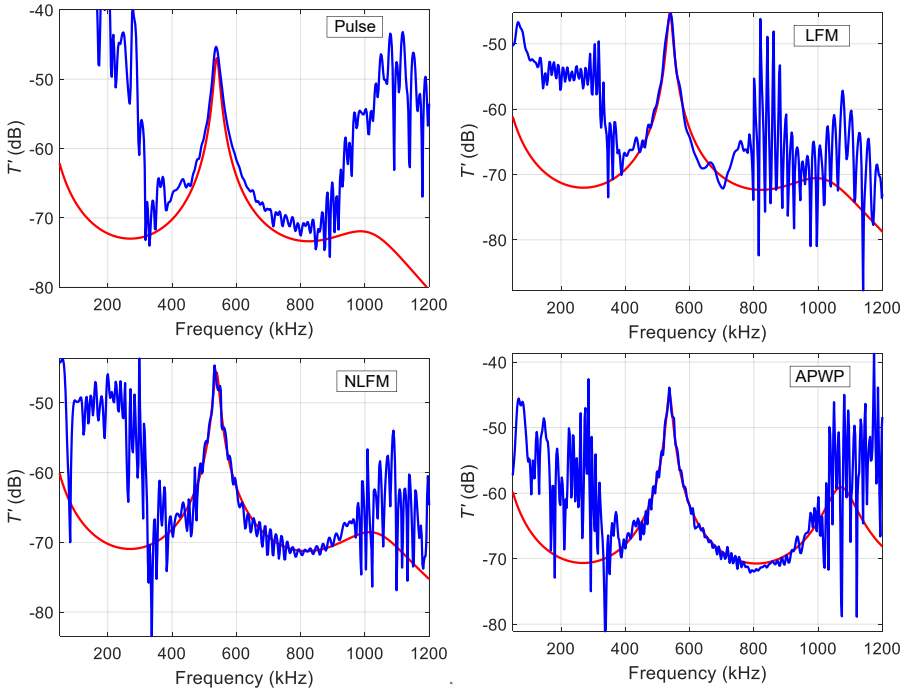

Fig. 15. Transmission magnitude for polycarbonate plate in case of different excitation signals: pulse (top left), LFM (top right), NLFM (bottom left) and APWP (bottom right).

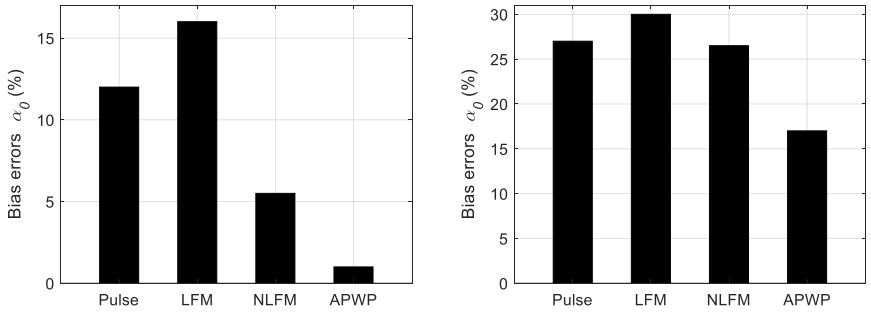

Fig. 16. Relative bias errors of attenuation estimation in case of four excitation signals (pulse, LFM, NLFM, APWP) for *Vitis Vinifera* (left) and polycarbonate (right) samples.

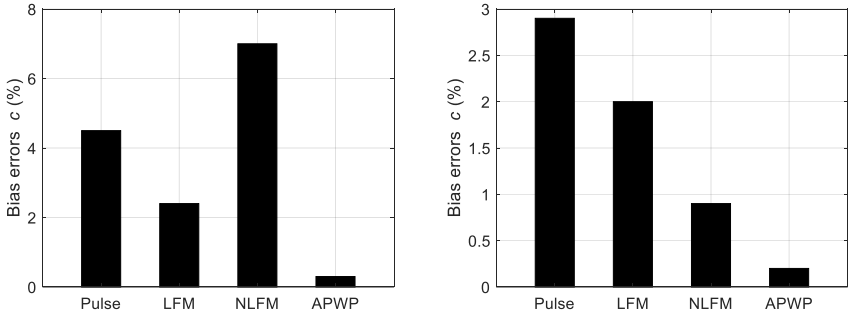

Fig. 17. Bias errors of ultrasound velocity estimation in case of four excitation signals (pulse, LFM, NLFM, APWP) for *Vitis Vinifera* (left) and polycarbonate (right).

sample are the highest in case of pulse excitation (2.9 %), followed by LFM (2 %) and NLFM (0.9 %). Again, use of APWP signal for excitation results in lowest ultrasound velocity estimation bias error (0.2 %).

Sample density ρ estimation bias errors are presented in (Fig. 18) for *Vitis vinifera* (left) and polycarbonate (right) samples.

Sample density ρ estimation error for *Vitis vinifera* sample is smallest in case of APWP excitation (2 %). NLFM signal also demonstrated acceptable performance, 4 % error, other signals resulted in much

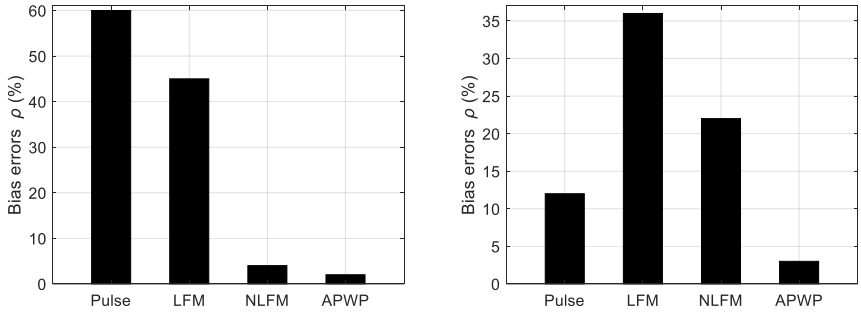

Fig. 18. Bias errors of sample density estimation of *Vitis Vinifera* (left) and polycarbonate (right) samples.

larger, 45 % (LFM) and 60 % (pulse) error. For polycarbonate sample, use of APWP for excitation resulted in lowest, 3 % error. Results obtained using LFM excitation had the largest (36 %) error. In case of NLFM excitation error was 22 %, pulse excitation resulted in 12 % error in polycarbonate sample density ρ estimation.

Sample thickness h estimation bias errors are presented in (Fig. 19) for *Vitis vinifera* (left) and polycarbonate (right) samples.

Sample thickness h estimation error for *Vitis vinifera* sample is smallest in case of APWP excitation (3 %), other signals resulted in much larger, around 30 % error. For polycarbonate sample situation is similar: use of APWP for excitation resulted in 25 % error, while other signals have more than 40 % error in sample thickness h estimation.

It can be concluded that spectral losses compensation with SNR equalization reduces the bias errors in NC-RUS measurements.

6. Conclusions

It has been demonstrated that the air-coupled resonance ultrasound spectroscopy is extremely demanding for high SNR and wide bandwidth. Application of matching layers on air-coupled transducer to improve the sensitivity and bandwidth produces uneven transduction sensitivity and electrical impedance over frequency range. It has been proven that not just signal spectrum but also noise spectral density are irregular.

Assumption, that the useable signal bandwidth (where acceptable SNR is achieved) defines the attainable resolution and parameters measurement range was made. It was proposed to replace the single pulse excitation with the programmable spectral shape spread spectrum signal to produce a uniform SNR within a passband. It has been shown that the use of spread spectrum signals allows to achieve the acceptable SNR over the range broader than transducer passband, attainable using pulse excitation. While −20 dB bandwidth in case of pulse excitation was 480 kHz, APWP excitation produced 670 kHz bandwidth.

It has been established that the unipolar excitation signals can be used to obtain the acceptable performance of spectral shaping. Use of unipolar excitation allows for simpler electronics.

The proposed scheme was tested within a NC-RUS framework for both leaf and polycarbonate sample measurements. Numerical simulations were performed for leaf measurements in order to have control over sample parameters. An experimental validation was conducted using a thin polycarbonate sample.

Both simulation and experiment results confirmed that use of uniform SNR signals (APWP) resulted in lowest bias error for all parameters estimation. In case of *Vitis Vinifera* leaf measurements, bias error in density estimation was 2 % with APWP signals while LFM resulted in 45 % and pulse in 60 % error. The polycarbonate sample velocity estimation error using APWP signal was 0.2 %, while LFM was 10 times higher (2 %); density estimation error for APWP was 3 %, but LFM resulted in 36 %, NLFM error was 22 %, pulse excitation resulted in 12 % error.

The application considered here was plant leaf and polycarbonate plate. However, the proposed scheme is applicable for other NC-RUS applications. The present APWP optimization uses full permutation. Possible improvement can be made by application of heuristic optimization algorithms. There are multiple reflections between ultrasonic transducers and sample which limit maximum signal length to 100 μs. If proper reverberation canceling or deconvolution solution is found results can be further improved by using very long signals. Future development could also include other optimization criteria.

CRediT authorship contribution statement

Muhammad Tayyib: Writing – original draft, Validation, Software, Methodology, Investigation. **Linas Svilainis:** Writing – review & editing, Supervision, Resources, Methodology, Funding acquisition, Conceptualization.

Declaration of competing interest

The authors declare the following financial interests/personal relationships which may be considered as potential competing interests: Linas Svilainis reports financial support was provided by Research

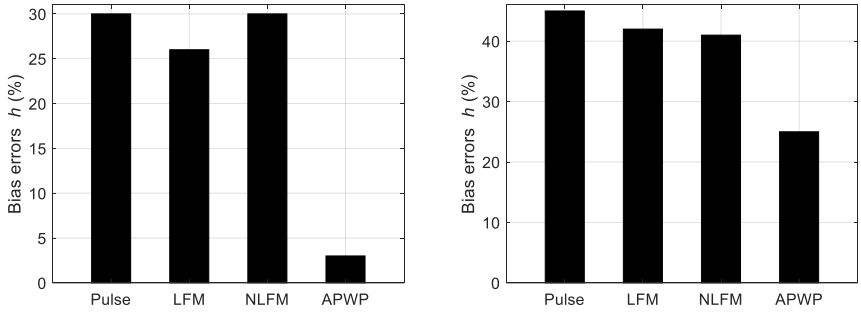

Fig. 19. Bias errors of sample thickness estimation of *Vitis Vinifera* (left) and polycarbonate (right) samples.

Council of Lithuania. If there are other authors, they declare that they have no known competing financial interests or personal relationships that could have appeared to influence the work reported in this paper.

Acknowledgment

This research was funded by a Grant No. S-MIP-23-133 from the Research Council of Lithuania.

Data availability

Data will be made available on request.

References

[1] Balakirev FF, Ennaceur SM, Migliori RJ, Maiorov B, Migliori A. Resonant ultrasound spectroscopy: the essential toolbox. Rev Sci Instrum 2019;90(12).
[2] Zadler BJ, Le Rousseau JH, Scales JA, Smith ML. Resonant ultrasound spectroscopy: theory and application. Geophys J Int 2004;156(1):154–69.
[3] Beardslee L, Shokouhi P, Ulrich TJ. Optimal measurement point selection for resonant ultrasound spectroscopy of complex-shaped specimens using principal component analysis. NDT E Int 2024;141:103000.
[4] Guo H, Lal A. Die-level characterization of silicon-nitride membrane/silicon structures using resonant ultrasonic spectroscopy. J Microelectromech Syst 2003;12(1):53–63.
[5] Bozek E, Williams CL, Rivière J, Shokouhi P. Nonlinear/linear resonance ultrasound spectroscopy (N/RUS) of additive-ly manufactured 316L stainless steel samples using in-contact and non-contact excitation. NDT E Int 2023;140:102948.
[6] Reed N, Corcoran J. Passive wall thickness monitoring using acoustic emission excitation. NDT E Int 2024;148:103241.
[7] Wang WX, Zhang J, Wilcox PD. Metallic material microstructure grain size measurements from backscattering signals in ultrasonic array data sets. NDT E Int 2025;149:103251.
[8] Alvarez-Arenas TEG, Soto DA. Characterization of mineral paper by air-coupled ultrasonic spectroscopy. Ultrasonics 2012;52(6):794–801.
[9] Quaegebeur N, Masson P, Berry A, Ardin C, D'Anglade PM. Ultrasonic non-destructive testing of cardboard tubes using air-coupled transducers. NDT E Int 2018;93:18–23.
[10] Farinas MD, Alvarez-Arenas TEG, Aguado EC, Merino MG. Non-contact ultrasonic inspection of cfrp prepregs for aeronautical applications during lay-up fabrication. In: IUS conference proceedings; 2013. p. 1586–9.
[11] Akseli I, Dey D, Cetinkaya C. Mechanical property characterization of bilayered tablets using nondestructive air-coupled acoustics. AAPS PharmSciTech 2010;11(1):90–102.
[12] Rossdeutscher J, Mechnich P, Flucht F, Shi Y, Jemmali R. Mechanical and microstructural assessment of inhomogeneities in oxide ceramic matrix composites detected by air-coupled ultrasound inspection. J Compos Sci 2021;5(11):286.
[13] Farinas MD, Sancho-Knapik D, Peguero-Pina JJ, Gil-Pelegrin E, Alvarez-Arenas TG. Contact-less, non-resonant and high-frequency ultrasonic technique: towards a universal tool for plant leaf study. Comput Electron Agric 2022;199.
[14] Haines NF, Bell JC, McIntyre PJ. The application of broadband ultrasonic spectroscopy to the study of layered media. J Acoust Soc Am 1978;64:1645.
[15] Kline RA. Measurement of attenuation and dispersion using an ultrasonic spectroscopy technique. J Acoust Soc Am 1984;76(2):498–504.
[16] Alvarez-Arenas TG. Simultaneous determination of the ultrasound velocity and the thickness of solid plates from the analysis of thickness resonances using air-coupled ultrasound. Ultrasonics 2010;50(2):104–9.
[17] Brekhovskikh LM, Godin OA. Acoustics of layered media I. Springer series on wave phenomena. Springer-Verlag; 1990.
[18] Alvarez-Arenas TG. A nondestructive integrity test for membrane filters based on air-coupled ultrasonic spectroscopy. IEEE Trans Ultrason Ferroelectrics Freq Control 2003;50:676–85.
[19] Alvarez-Arenas TG, Farinas MD, Ginel A. Fast and non-destructive ultrasonic test for face masks. Ultrasonics 2021;117:106556.
[20] Aleksandrovas A, et al. Miniature air coupled ultrasound data acquisition system for field application of resonance spectroscopy. In: IEEE int ultrason symp; 2022. p. 1–3.
[21] Khuri-Yakub BT, Kim JH, Chou CH, Parent P, Kino GS. A new design for air transducers. In: IEEE int ultrason symp; 1988.
[22] Electroacoustics. Measurement microphones - Part 3: primary method for free field calibration of laboratory standard microphones by the reciprocity technique. IEC 61094-3:2016. Int Elect Commission 2020.
[23] Rasmussen K. Calculation methods for the physical properties of air used in the calibration of microphones. Technical University of Denmark; 1997. Report PL-11b.
[24] Rathod VT. A review of acoustic impedance matching techniques for piezoelectric sensors and transducers. Sensors 2020;20(14):4051.
[25] Alvarez-Arenas TG. Acoustic impedance matching of piezoelectric transducers to the air. IEEE Trans Ultrason Ferroelectrics Freq Control 2004;51(5):624–33.
[26] Gu JJ, Zhao Q, Yin B, Zhou H, Qu S. Lowering the sound transmission loss of impedance-matching structures: data-driven optimization assisted with a priori knowledge. Mater Des 2023;232:112091.
[27] Gudra T, Opielinski KJ. Influence of acoustic impedance of multilayer acoustic systems on the transfer function of ultrasonic airborne transducers. Ultrasonics 2002;40(8):457–63.
[28] Alvarez-Arenas TG, Diez L. Novel impedance matching materials and strategies for air-coupled piezoelectric transducers. IEEE Sensors 2013:1494–7.
[29] Farinas MD, et al. Instantaneous and non destructive relative water content estimation from deep learning applied to resonant ultrasonic spectra of plant leaves. Plant Methods 2019;15:128.
[30] Alvarez-Arenas TG, Sancho-Knapik D, Peguero-Pina JJ, Gil-Pelegrín E. Noncontact and noninvasive study of plant leaves using air-coupled ultrasounds. Appl Phys Lett 2009;95(9):193702.
[31] Folkestad T, Mylvaganam KS. Chirp excitation of ultrasonic probes and algorithm for filtering transit times in high-rangeability gas flow metering. IEEE Trans Ultrason Ferroelectrics Freq Control 1993;40(3):193–215.
[32] Pollakowski H, Ermert H, Von Bernus L, Schmeidl T. The optimum bandwidth of chirp signals in ultrasonic applications. Ultrasonics 1993:417–20.
[33] Dantas TM, Cpsta-Feliz RPB, Machado JC. Nonlinear frequency modulated excitation signal and modified compressed filter for improved range resolution and side lobe level of ultrasound echoes. Appl Acoust 2018;30:238–46.
[34] Toh R, Motooka S. Target ranging using ultrasonic sensitivity compensated signal and pulse compression. Jpn J Appl Phys 2009;48(7S):07GB09.
[35] Svilainis L, Aleksandrovas A. Application of arbitrary pulse width and position trains for the correlation sidelobes reduction for narrow band transducers. Ultrasonics 2013;53(7):1344–8.
[36] Svilainis L, Rodriguez-Martinez A, Chaziachmetovas A, Aleksandrovas A. Ultrasound transmission spectral compensation using arbitrary position and width pulse sets. IEEE Trans Instrum Meas 2018;67(8):1778–85.
[37] Rodriguez-Martinez A, et al. On the optimization of spread spectrum chirps into arbitrary position and width pulse signals. Application to ultrasonic sensors and systems. IEEE Access 2022;10:2013–27.
[38] Sherrity S, et al. Accurate equivalent circuit for the unloaded piezoelectric vibrator in the thickness mode. J Phys D Appl Phys 1997;30:2354–63.
[39] Svilainis L, Chaziachmetovas A, Alvarez-Arenas TG. Ultrasonic air coupled transducer output impedance measurement technique. Elektron ir Elektrotech 2019;25(1):18–25.
[40] Svilainis L, Dumbrava V, Kybartas D. Evaluation of the ultrasonic preamplifier noise voltage density. J Cricuits Syst Comput 2014;23(1).
[41] Tsuji K, Norisuye T, Nakanishi H, Tran-Cong-Miyata Q. Simultaneous measurements of ultrasound attenuation, phase velocity, thickness, and density spectra of polymeric sheets. Ultrasonics 2019;99:105974.
[42] Nakutis Ž, Kaškonas P, Liaukonis D, Svilainis L. Air-coupled ultrasound spectroscopy air parameters compensation technique. IEEE Sens J 2024;24(8):12667–75.